



Journal homepage:
<http://www.bsu.edu.eg/bsujournals/JVMR.aspx>
Online ISSN: 2357-0520 Print ISSN: 2357-0512



Original Research Article

Cross-sectional Anatomy, Magnetic Resonance Imaging and Computed Tomography of Fetlock Joint in Camel

Ibrahim, A.H.*, Adam, Z.E. and Mohamed G. Tawfik

Anatomy and Embryology Department, Faculty of Veterinary Medicine, Beni-Suef University, Beni-Suef 62511, Egypt

ABSTRACT

The current study aimed to describe the normal cross-sectional anatomy, magnetic resonance imaging, and computed tomography of the fetlock joint in adult healthy dromedary camel. This study was carried out on twelve fetlock joints of the fresh cadavers from three camels. The gross examination of these camels revealed that they were normal with no orthopedic abnormalities. The cadaveric fetlock joints (n=12) were scanned using a computed tomographic (CT) scanner and a 1 Tesla MRI scanner. Then the joints were injected with a colored latex and sectioned into transverse, dorsal, and sagittal slices. Cross-anatomical sections were correlated with their corresponding CT and MR images for evaluation of the normal relevant anatomical structures that appeared with different signal intensities on the CT and MRI scans. The current investigation revealed that all the major soft tissue structures in the fetlock joint of the dromedary camel were clearly visualized on both CT and MR scans, except the short and the cruciate sesamoidean ligaments that could not be identified on both the CT and MR images. The anatomical sections with their corresponding CT and MR images obtained in this study could be used as a reference for subsequent clinical diagnosis and the interpretation of fetlock joint pathologies in dromedary camel.

ARTICLE INFO

Received: 29/04/ 2019
Accepted: 30/07/2019
Published online: 02/08/2019

Keywords:

Anatomy, Computed Tomography (CT), Camel, Fetlock joint, Magnetic Resonance Imaging

*Corresponding author: Ibrahim, A.H. Anatomy and Embryology Department, Faculty of Veterinary Medicine, Beni-Suef University, Beni-Suef 62511, Egypt. E-mail address: d.azzamohamed88@gmail.com

1. Introduction

Camel is adapted to the hard climatic conditions of the desert and has the capability to survive and produce under hard environmental conditions (Sadegh et al. 2007). Concurrently, it is used as an important source of milk, meat and hide especially in the developing countries (Ahmad et al. 2010). Moreover, the camel is considered an essential economy source in the Gulf region through the camel racing sports and tourism (Farah and Fischer 2004).

Lameness is a serious worldwide problem due to its negative economic impact on the dairy farms (Solano et al. 2015). Moreover, the camel has a different pattern of lameness when compared to the bovine and equine, because of its peculiar anatomy and biomechanics (Al-Juboori 2013). These instances require awareness of the normal anatomical structures and developing of the modern diagnostic imaging techniques for the identification and evaluation of the orthopedic problems.

Recently, there is a growing awareness for the use of the computed tomography (CT) and magnetic resonance imaging (MRI) as valuable diagnostic imaging modalities in veterinary practices (Bienert and Stadler 2006; Nuss et al. 2011). However, their limited accessibility, high costs and the need for animal general anesthesia diminish the use of these techniques in veterinary practices (Arencibia et al. 2000). Nevertheless, improvement in availability and accessibility of these tools increases the demand for their use in animals (Pollard and Puchalski 2011). These techniques are not only used for diagnostic purposes, but also can be used in several biometric researches and measurements (Onar et al. 2002). Even though many CT and MRI studies had been done on different joints of the animal digits (Badawy 2011; El-Shafey and Abd Al-Galil 2012; El-Shafey and Kassab 2012; El-Nahas et al. 2015 in camel; Raji et al. 2008 and 2009; AlAkraa et al. 2014 in bovine; Sampson et al. 2005; Sampson and Tucker 2007 in horse). More details on the cross sectional anatomy of the fetlock joint of the dromedary camel in correspondence to the CT and MRI are still needed.

The present study aimed to provide a comprehensive detailed anatomic reference on the cross-sectional anatomy, CT and MRI of the fetlock joint in dromedary camel to be used as a helpful reference for the interpretation and evaluation of the musculoskeletal disorders of the fetlock joint in camels.

2. Materials and methods

2.1. Animals

CT and MRI examination were performed on twelve fetlock joints (right and left) of the fresh cadavers from three dromedary camels (age 2-4 years, weighed about 350-500 kg). These cadaveric limbs (fore and hind limbs) were obtained from the local slaughter-house at Beni-Suef Governorate. The camels were grossly normal with no fetlock joint disorders.

2.2. Magnetic Resonance Imaging (MRI)

Distal limbs (n=12) were positioned with their palmar/plantar aspects as the dependent portion and their long axis perpendicular to the examination table. T1-weighted MR images (TR = 1900 ms, TE = 2.74 ms, slice thickness = 2mm) were acquired in transverse, sagittal, and dorsal planes using a 1 Tesla

MR scanner (Philips Medical system Intera, 1T MRI; Philips GmbH, Hamburg, Germany). This examination was done within three hours after slaughtering.

2.3. Computed Tomography Imaging (CT)

Distal limbs were placed on the examination table as done in the MRI study. Toshiba Alexion CT scanner was used for obtaining the bone and soft tissue windows CT scans in transverse, dorsal, and sagittal planes. The acquisition settings were 120 KV and 250 MA with 2mm slice thickness.

2.4. Preparation of the cross-anatomical sections

The scanned specimens (n=12) were injected with a colored gum-milk latex. The needle was introduced into the dorsal pouches of the fetlock joint abaxial to the tendinous portions of the digital extensor tendons. The limbs were frozen at -18°C for one week. Then sectioned into transverse

(forelimbs=2, hind limbs=2), dorsal (forelimbs=2, hind limb=2) and sagittal (forelimbs=2, hind limbs=2) slices starting about 10 cm dorsal to the fetlock joint till the middle of the first phalanx in 1cm slice thickness using an electric band saw. All anatomic sections were gently cleaned using tap water and then photographed. The anatomical sections were inspected, identified and selected in correlation to their corresponding CT and MR images.

2.5. Comparison of the cross-anatomical sections with CT and MR images

The cross-anatomical sections of the fetlock joint were compared to their corresponding CT and MR images on the basis of the shape, location and tissue density properties.

For evaluation of the most clinically relevant anatomical structures of the fetlock joint in dromedary camel of the same specimens, six CT and MR images were selected to be representative for the anatomical structures (**Fig. 1**) in their matched anatomical sections, one in the sagittal plane, two in the dorsal planes and three in the transverse planes.

3. Results

The obtained anatomical cross sections were selected and compared with their corresponding CT and MR images in a sagittal plane (**Fig. 2**), dorsal planes (**Figs. 3, 4**) and transverse planes (**Figs. 5-7**). No significant morphological or topographical variations were observed between the fetlock joints of the fore and hind limbs, or between the right and left contralateral limbs.

3.1. Magnetic Resonance Imaging (MRI)

Articular cartilages were clearly recognized from the surrounding bony structures as a thin layer of high signal intensity (**Figs. 2, 4**). Subchondral bone appeared as a thin plate of a low signal intensity and could be easily differentiated from the articular cartilage at the proximal extremity of each bone (**Figs. 2, 4**). Cancellous bone could be visualized at the extremities of each bone with a heterogeneous high signal intensity (**Figs. 2, 4**). Cortical bone had a low signal intensity, while the medulla had a high signal intensity (**Figs. 2, 4**). However, the

trabecular pattern of the bones could not be differentiated on the obtained MR images. Proximal sesamoid bones were best recognized on the transverse MR images (**Fig. 6**).

Soft tissue structures were clearly visualized in all MR images with variable signal intensities. Extensor tendons could be recognized on the MR images included; the lateral and common digital extensor tendons. These tendons had homogenous low signal intensities. Margins of these tendons were well-defined by the surrounding fascia that appeared as an intermediate signal intensity. Extensor tendons were best evaluated on the transverse MR images as three narrow strips on the dorsal aspect of the distal end of the metacarpus/metatarsus (**Figs. 5-6**).

At the level of the proximal phalanges, the extensors appeared as four structures indicated the division of the lateral limb of the common digital extensor tendon into two branches which could be visualized as small oval structures on the dorsomedial aspect of each digit (**Fig. 7**).

On the palmar/plantar aspect of the distal end of the metacarpus/metatarsus, the inter-osseous muscle (suspensory ligament) could be clearly visualized as an elongated structure with had a low signal intensity deep to the digital flexor tendons at a level about 4cm proximal to the fetlock joint, this muscle appeared as four oval structures representing the axial and abaxial proximal sesamoidean ligaments on the transverse MR images (**Fig. 5**). However, the inter-osseous muscle and its branches were best evaluated on the dorsal MR images at the level of the sesamoid bones (**Fig. 2**). Moreover, the branches of the inter-osseous muscle could be depicted on the sagittal MR images (**Fig. 2**).

Digital flexor tendons appeared with homogenous low signal intensity structures surrounded by digital tendon sheath which had a low signal intensity. On the transverse MR images, superficial digital flexor tendon (SDFT) appeared as an incomplete ring around the oval-shaped deep digital flexor tendon (DDFT) till the level of the

proximal extremity of the first phalanx (**Figs. 5-7**). On the dorsal MR images, the SDFT appeared as two branches on both sides of the DDFT, and then it changed its position to be deep to DDFT (**Fig. 3**). This reposition of the flexor tendons could be also recognized on the sagittal MR images (**Fig. 2**). Moreover, the manica flexoria of the SDFT had a high signal intensity that was best recognized on the transverse and dorsal MR images (**Figs. 3, 5**).

Joint capsules of the fetlock joint appeared as low signal intensities and the margins of these capsules were clearly outlined as a thin line of intermediate signal intensity on the sagittal, dorsal, and transverse MR images (**Figs. 2, 4, 6, 7**). However, the ligaments of this joint were well-defined and clearly outlined on the transverse and dorsal MR images as heterogeneous intermediate signal intensities (**Figs. 3-7**). While the straight sesamoidean ligament and the annular ligament could be identified on the sagittal MR images (**Fig. 2**). Ligaments of the fetlock joint that could be clearly identified on the obtained MR images included; the suspensory, collateral, collateral sesamoidean, palmar/plantar and straight sesamoidean ligaments. While the short and cruciate sesamoidean ligaments could not be defined.

3.2. Computed Tomography Imaging

The bone window provided an excellent delineation between the cortical and subcortical tissues as well as the bone medulla with a clear differentiation of the trabecular patterns. This medulla appeared as hypo dense black colored area. Diaphysis, condyles, sagittal ridges, proximal sesamoid bones, and phalanges appeared as hyper dense with smooth margins on the transverse, dorsal, and sagittal CT images (**Figs. 2-7**).

In soft tissue window, bones appeared as hyper dense structures, while the soft tissues were depicted with variable densities. On the dorsal aspect of the fetlock joint, extensor tendons; lateral digital extensor as well as the medial and lateral limbs of the common digital extensor were visualized as hyper dense structures compared with the surrounded hypodense connective tissues. These tendons were best recognized on the

transverse CT images as three narrow strips on the dorsal aspect of the metacarpus/metatarsus (**Fig. 5**). At the level of the proximal phalanx, these extensors appeared as four structures indicating the division of the lateral limb of the common digital extensor tendon into two branches that appeared as small oval structures on the dorsomedial aspect of the limb (**Figs. 6-7**). On the palmar/plantar aspect of the distal end of the metacarpus/metatarsus, the inter-osseous muscle (suspensory ligament) could be clearly visualized at a level about 4cm proximal to the fetlock joint as four oval structures representing the axial and abaxial proximal sesamoidean ligaments on the transverse CT images (**Fig. 5**). However, the inter-osseous muscle and its branches were best evaluated on the dorsal CT images at the level of the sesamoid bones (**Fig. 3**). Moreover, the branches of the inter-osseous muscle could be depicted on the sagittal CT images (**Fig. 2**).

Digital flexor tendons could be recognized as hyper dense structures surrounded by hypodense connective tissues on the palmar/plantar aspects of the fetlock joint on the transverse, dorsal, and sagittal CT images. On the transverse CT images, SDFT appeared as an incomplete ring around oval-shaped DDFT till the level of the proximal extremity of the first phalanx (**Figs. 5-7**). On the dorsal CT images, SDFT appeared as two branches on both sides of the DDFT, and then it changed its position to be deep to the DDFT (**Fig. 3**). This reposition of the flexor tendons could be also recognized on the sagittal CT images. Manica flexoria appeared as a well-defined hypodense structure on the transverse and dorsal CT images (**Figs. 2, 3, 5**).

Joint capsule of the fetlock joint appeared as a hypodense structure on the sagittal (**Fig. 2**), dorsal (**Fig. 4**) and transverse (**Figs. 5-7**) CT images. However, the ligaments of this joint were well-defined on the transverse and dorsal CT images as hyper dense structures with surrounding hypodense connective tissues (**Figs. 4-7**). While the straight sesamoidean and annular ligaments could be identified on the sagittal CT images (**Fig. 2**). On CT images, the ligaments of the fetlock joint could be clearly identified included; the suspensory,

collateral, collateral sesamoidean, palmar/plantar, and the straight sesamoidean ligaments. While the short and cruciate sesamoidean ligaments could not be recognized.

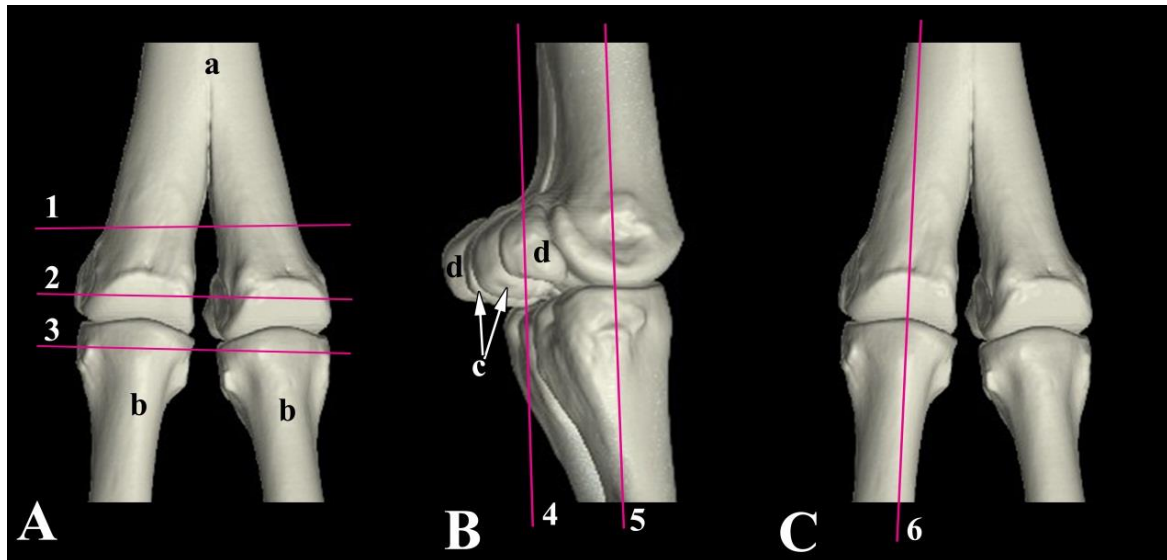


Fig. 1. Three dimensional reconstructed computed tomographic views of the fetlock joint of the dromedary camel. Numbered planes indicated the approximate levels of the cross-anatomical sections and their corresponding magnetic resonance imaging and computed tomographic depictions. **A.** Dorsal view showing the selected planes for the transverse sections (**1-3**); **B.** Lateral view showing the selected planes for the dorsal sections (**4- 5**); **C.** Dorsal view showing the selected planes of the sagittal sections (**6**); **a.** Metacarpus/ metatarsus; **b.** First phalanx; **c.** Axial sesamoid bones; **d.** Abaxial sesamoid bones.

Fig. 2. Sagittal images of the right fore fetlock joint of the dromedary camel (level 6 as indicated in Fig. 1). **A.** Sagittal anatomical section; **B.** Magnetic resonance image; **C.** Bone window computed tomography image; **D.** Soft tissue window computed tomography image. **1.** Metacarpus; **2.** First phalanx; **3.** Proximal sesamoid bone; **4.** Articular cartilage; **5.** Cancellous bone; **6.** Cortical bone; **7.** Subchondral bone; **8.** Suspensory ligament; **9.** Deep digital flexor tendon; **10.** Superficial digital flexor tendon; **11.** Manica flexoria; **12.** Annular ligament; **13.** Straight sesamoidean ligament; **14.** Dorsal synovial pouch of fetlock joint; **15.** Palmar synovial pouch of fetlock joint; **16.** Palmar synovial pouch of pastern joint.

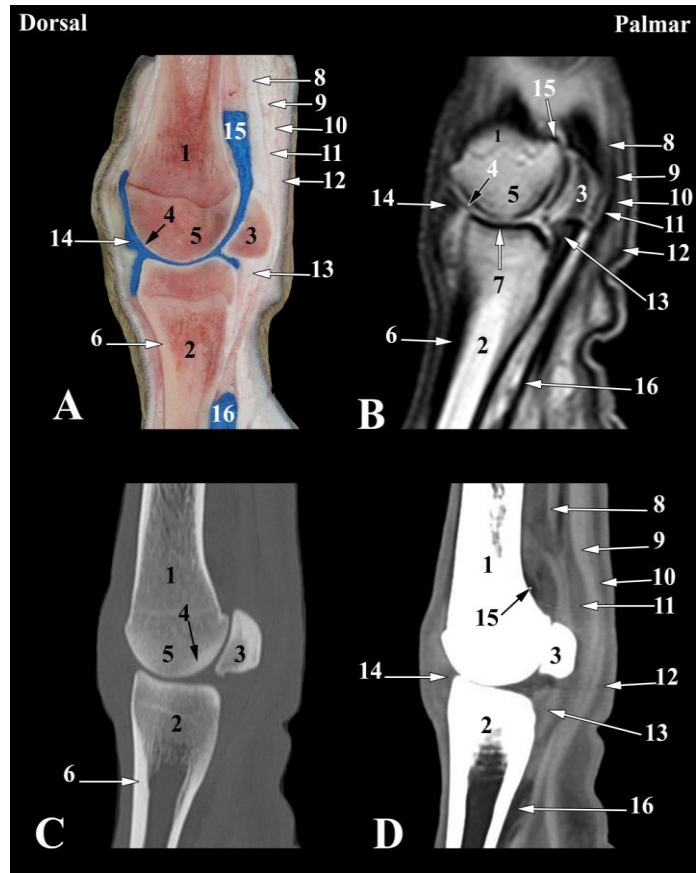
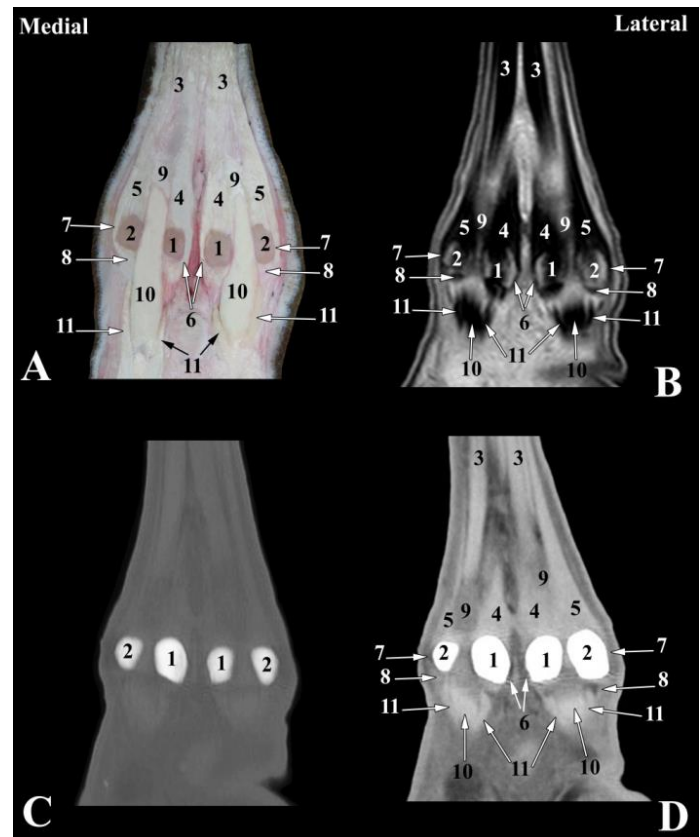


Fig. 3. Dorsal images of the right hind fetlock joint of the dromedary camel at the level of the proximal sesamoid bones (Level 4 as indicated in Fig. 1). **A.** Dorsal anatomical section; **B.** Magnetic resonance image; **C.** Bone window computed tomography image; **D.** Soft tissue window computed tomography image: **1.** Axial sesamoid bones; **2.** Abaxial sesamoid bones; **3.** Inter-osseous muscle; **4.** Axial limbs of inter-osseous muscle; **5.** Abaxial limbs of inter-osseous muscle; **6.** Axial collateral sesamoidean ligaments; **7.** Abaxial collateral sesamoidean ligaments; **8.** Straight sesamoidean ligaments; **9.** Manica flexoria; **10.** Deep digital flexor tendon; **11.** Superficial digital flexor tendon.



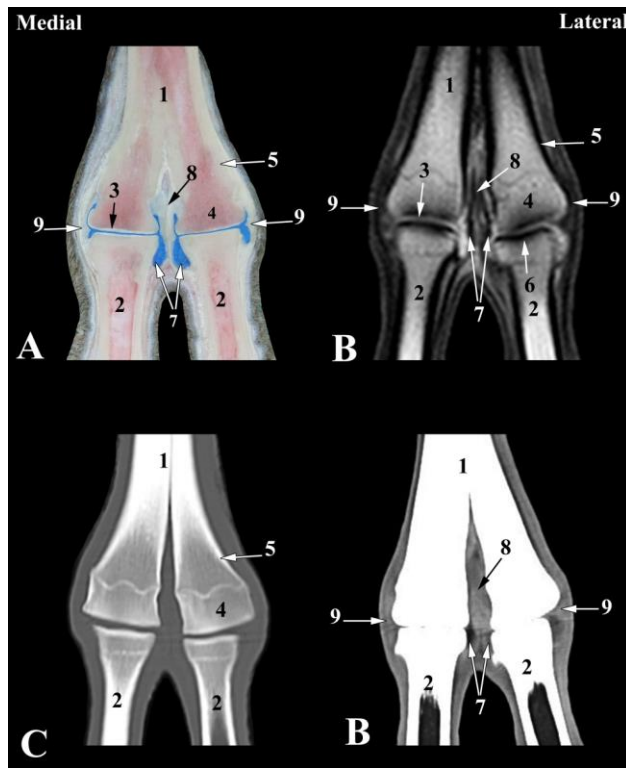


Fig. 4. Dorsal images of the fetlock joint of the dromedary camel at the level of the collateral ligaments attachment (**Level 5 as indicated in Fig. 1**). **A.** Dorsal anatomical section; **B.** Magnetic resonance image; **C.** Bone window computed tomography image; **D.** Soft tissue window computed tomography image. **1.** Metacarpus; **2.** Proximal phalanx; **3.** Articular cartilage; **4.** Cancellous bone; **5.** Cortical bone; **6.** Subchondral bone; **7.** Joint cavity of fetlock joint; **8.** Axial collateral ligaments of fetlock joint; **9.** Abaxial collateral ligaments of fetlock joint.

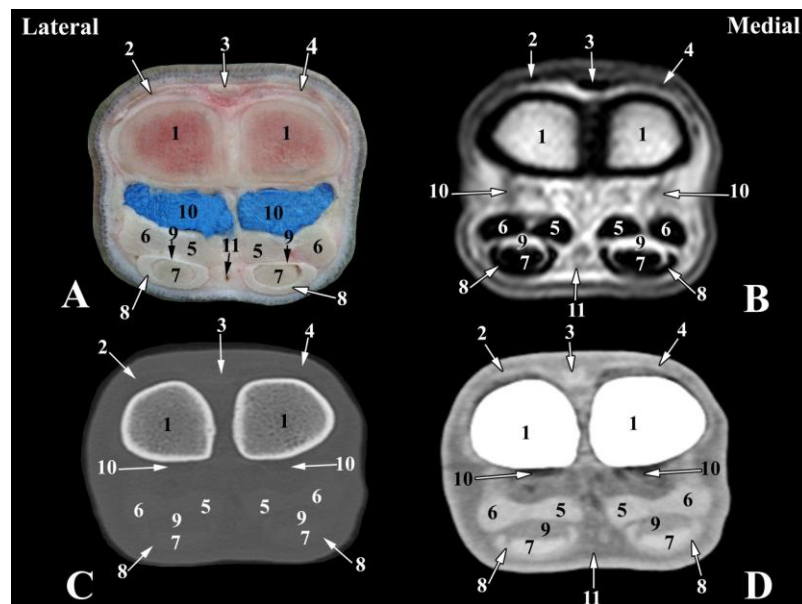


Fig. 5. Transverse images of the right fore fetlock joint of the dromedary camel at the level of the metacarpal trochlea (**Level 1 as indicated in Fig. 1**). **A.** Transverse anatomical section; **B.** Magnetic resonance image; **C.** Bone window computed tomography image; **D.** Soft tissue window computed tomography image. **1.** Metacarpus; **2.** Lateral digital extensor tendon; **3.** Lateral limb of the common digital extensor tendon; **4.** Medial limb of the common digital extensor tendon; **5.** Axial limbs of the inter-osseous muscle; **6.** Abaxial limbs of the inter-osseous muscle; **7.** Deep digital flexor tendon; **8.** Superficial digital flexor tendon; **9.** Manica flexoria; **10.** Palmar synovial pouch of the fetlock joint; **11.** Common palmar digital artery.

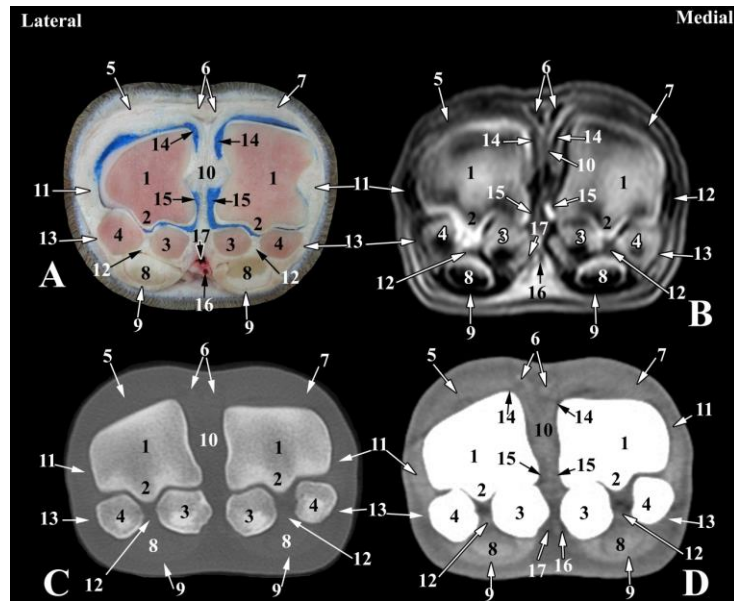


Fig. 6. Transverse images of the right fore fetlock joint of the dromedary camel at the level of the proximal sesamoid bones (**Level 2 as indicated in Fig. 1**). **A.** Transverse anatomical section; **B.** Magnetic resonance image; **C.** Bone window computed tomography image; **D.** Soft tissue window computed tomography image. **1.** Metacarpus; **2.** Palmar sagittal ridge; **3.** Axial sesamoid bones; **4.** Abaxial sesamoid bones; **5.** Lateral digital extensor tendon; **6.** Lateral limb of the common digital extensor tendon; **7.** Medial limb of the common digital extensor tendon; **8.** Deep digital flexor tendon; **9.** Superficial digital flexor tendon; **10.** Axial collateral ligaments of the fetlock joint; **11.** Abaxial collateral ligaments of the fetlock joint; **12.** Palmar ligament of the fetlock joint; **13.** Collateral sesamoidean ligaments; **14.** Dorsal synovial pouch of the fetlock joint; **15.** Palmar synovial pouch of the fetlock joint; **16.** Common palmar digital artery; **17.** Common palmar digital vein.

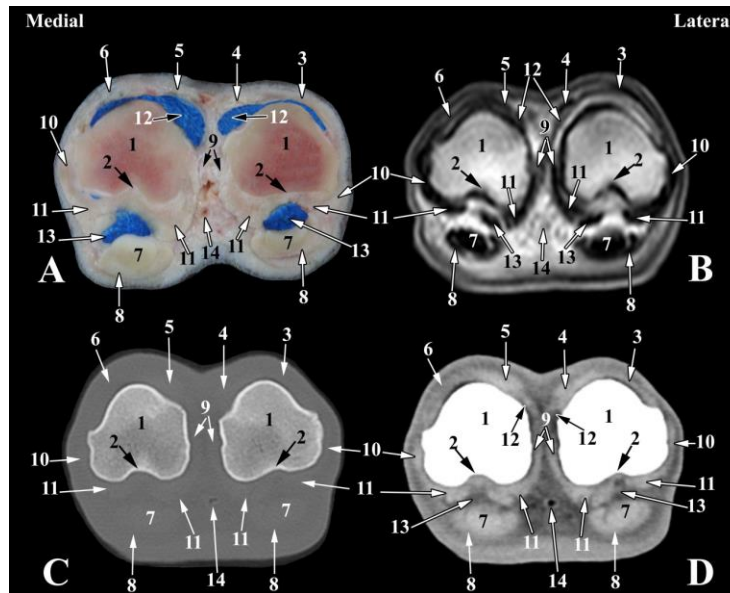


Fig. 7. Transverse images of the left hind fetlock joint of the dromedary camel at the level of the proximal phalanx (**Level 3 as indicated in Fig. 1**). **A.** Transverse anatomical section; **B.** Magnetic resonance image; **C.** Bone window computed tomography image; **D.** Soft tissue window computed tomography image. **1.** Proximal phalanx; **2.** Trochlear fovea of the proximal phalanx; **3.** Lateral digital extensor tendon; **4.** Lateral branch of the lateral limb of the common digital extensor tendon; **5.** Medial branch of the lateral limb of the common digital extensor tendon; **6.** Medial limb of common digital extensor tendon; **7.** Deep digital flexor tendon; **8.** Superficial digital flexor tendon; **9.** Axial collateral ligaments; **10.** Abaxial collateral ligaments; **11.** Straight sesamoidean ligaments; **12.** Dorsal synovial pouch of the fetlock joint; **13.** Plantar synovial pouch of the fetlock joint; **14.** Common plantar digital artery.

4. Discussion

The compared anatomical cross sections with their corresponding CT and MR images provided detailed views for the normal relevant structures of the fetlock joint in dromedary camel. These images could be used as a normal anatomic reference during the diagnosis of the musculoskeletal disorders in this particular region. CT and MRI were excellent imaging modalities used for scanning of the fetlock joint in camel. These modalities permitted visualization of the clinically relevant structures in three planes and serial slices allowing evaluation of these structures at several angles. Moreover, using latex injected joint cavities allowed a precise description of the anatomical features of this joint, and gave a standard clinical reference for the position and shape of the normal anatomical structures. CT images were acquired with minimal slice thickness and interstice space providing an accurate spatial resolution and decrease partial volume artifacts, as well as a T1-weighted MRI sequence was adjusted with minimal slice thickness at a high acquisition speed; these acquisitions allowed more detailed anatomical structures to be feasible for practical clinical imaging (Smith et al. 2011).

Due to the peculiar anatomy of the distal limb in dromedary camel and high risk of lameness which may affect the draft ability (Al-Juboori 2013). Using a high definitive diagnostic technique is very important. However, radiography is the main technique for evaluation of the musculoskeletal disorders due to its entire differentiation of the bony structures, ready accessibility and low cost (Kinns and Nelson 2010), but the normal radiography technique causes superimposition and overlapping of the soft tissues (Van Der Vekens et al. 2011). Moreover, the non-invasive ultrasonography technique cannot penetrate the hard structures such as the bones and cartilages (Samii et al. 1998), so it gives a small field of view and each structure have to be depicted separately, and a cross-sectional study through the entire digit is difficult (Denoix et al. 1993). Nevertheless, ultrasonography is used well for visualization of separate ligaments and tendons (Lisher and Walliser 2005). Therefore, CT and MRI are

excellent diagnostic techniques providing a better evaluation of soft tissues (Raji et al. 2008; Seddek et al. 2014; Abedallaah et al. 2015; Hagag and Tawfiek 2018). Moreover, these modalities give good spectrum views of the cross-sectional imaging helping in the diagnosis of the abnormalities and the extent of the lesions (Raji et al. 2009). Although, CT permits high detailed osseous structures and can distinguish bony changes before they are radiographically or clinically apparent (Young et al. 2007), and can be used for evaluation of the soft tissue structures (Raji et al. 2008; Seddek et al. 2014). However, MRI can simultaneously permit imaging of the bones and soft tissues with a higher soft tissue contrast than CT, and no risk of ionizing radiation (Hagag and Tawfiek 2018). In agreement with El-Nahas et al. (2015) in camel and Hagag and Tawfiek (2018) in cattle, the CT bone window allowed differentiation between the cortex and medulla. Moreover, the present study showed that the CT bone window images provided more delineated trabecular pattern than the MR images.

The bone elements of the distal end of the metacarpus/metatarsus, proximal end of the first phalanx and the sesamoid bones were outlined in this study using CT as hyper dense structures with smooth margins. Similar results were observed in camel (Badawy, 2011); buffalo and camel (El-Shafey and Kassab, 2012); cattle (Raji et al. 2008; Hagag and Tawfiek, 2018); cattle and buffalo (Al-Akraa et al. 2014). Moreover, the medulla of these bones appeared hypodense and black in color, similarly with the results of Badawy (2011) in camel and Raji et al. (2008) in cattle.

Using the MRI scanning in the current study for evaluation of the articular cartilages, cortical bone, subchondral bone, cancellous bone and these structures were clearly outlined. Articular cartilages were evaluated on the MRI not on the CT images, where they were recognized from the surrounding bony structures as thin layers of high signal intensities. Similar findings were reported by Hagag and Tawfiek (2018) in cattle. On the other hand, the articular cartilage could be observed

using the CT in horse (**Vanderperren et al. 2008**). **Cohen et al. (1999)** attributed this difficult imaging to the markedly curved articular surfaces of the distal limb and the too thin cartilages for the spatial resolution in clinical MRI.

Using MRI in this study, the subchondral bone appeared as a thin plate of low signal intensity and could be easily differentiated from the articular cartilage at the proximal extremity of each bone. Moreover, the cancellous bone could be visualized at the extremity of the first phalanx with a heterogeneous high signal intensity and the cortical bone had a low signal intensity. Similar findings were observed by **Hagag and Tawfik (2018)** in cattle.

The present study showed that the medulla of the distal end of the metacarpus/metatarsus and the proximal end of the first phalanx had high signal intensities on the MRI and it appeared as hypodense and black colored structures on the CT images. On contrary to that it appeared with a low signal intensity in camel (**El-Shafey and AbdAl-Galil 2012**) and in cattle (**Raji et al. 2009**). While it appeared as a dark shade in the CT images in camel (**Badawy 2011**) and in cattle (**Raji et al. 2008**).

The current study revealed that all the major soft tissue structures in the distal limb of the dromedary camel were clearly visualized on both CT and MR images. However, it was difficult to identify the cruciate and the short sesamoidean ligaments on the CT and MR images, similar to the finding by **El-Shafey and Kassab (2012)**, **El-Shafey and Sayed-Ahmed (2012)** and **El-Shafey and Abd Al-Galil (2012)** in camel and **Hagag and Tawfik (2018)** in cattle. However, the two ligaments were only identified using the CT images including; the collateral ligaments and the collateral sesamoidean ligaments (**El-Nahas et al. 2015** in camel). While, all ligaments of the fetlock joint in horse could be outlined and recognized on the CT images except the collateral sesamoidean and the short distal sesamoidean ligaments (**Vanderperren et al. 2008**).

The present study and **Hagag and Tawfik (2018)** in cattle observed that the ligaments of the fetlock joint were visualized as heterogeneous intermediate signal intensities using the MR imaging. While, these ligaments were well-defined on the CT images as hyper dense structures with the surrounding hypodense connective tissues, similar to the findings of **El-Nahas et al. (2015)** in camel.

The extensor and flexor tendons were clearly outlined in cross anatomical sections and their corresponding MR and CT images in the current study. However, these tendons could be demonstrated in the cross anatomical sections only after dissection of the intervening fascia (**El-Shafey and Abdel Al-Galil 2012** in camel and **El-Shafey and Sayed-Ahmed 2012** in camel and buffalo). In agreement with **Hagag and Tawfik (2018)** in cattle, these tendons appeared as hyper dense structures with the surrounding hypodense connective tissue on the CT images, while they were visualized on the MR images as homogenous low signal intensities. Moreover, the deep digital flexor tendon was depicted on the CT images by **El-Nahas et al. (2015)** in camel as a hyper dense structure. In addition to that on the MR images, the SDFT appeared as rounded structure with a low signal intensity, and the DDFT appeared as oval shaped structure with a low signal intensity and clear outlines (**El-Shafey and Abd Al-Galil 2012** in camel). Moreover, the present study and **Hagag and Tawfik (2018)** in cattle depicted the digital sheath as a thin layer of a low signal intensity on the MR images. Moreover, this sheath was visualized on the CT images as a hypodense connective tissue surrounding the digital flexor tendons, similar to the results of **Puchalski et al. (2007)** in horse. Moreover, the current study permitted a detailed visualization of the manica flexoria in gross anatomical sections, CT, and MR images. This structure was depicted, in this study, with a high signal intensity that was best recognized on the transverse and dorsal MR images, while it appeared as a well-defined hypodense structure on the transverse and dorsal CT images. This manica flexoria is clearly visible on the CT images surrounding the deep digital flexor tendon proximal to the fetlock joint of the horse (**Vanderperren et al. 2008**). On the other

hand, it is demonstrated only in cross sectional anatomy of the buffalo, while in camel it could not be visualized either in cross anatomical sections or on the CT images (El-Shafey and Kassab 2012 and El-Shafey and Sayed-Ahmed 2012).

The inter-osseous muscle was clearly recognized in this study in gross anatomical sections, CT, and MR images, where it appeared as a hyper dense structure on the CT images and it had a low signal intensity on the MR images. Moreover, this muscle appeared as an elongated structure deep to the digital flexor tendons, while, at about 4cm proximal to the fetlock joint, this muscle appeared as four oval structures representing the axial and abaxial proximal sesamoidean ligaments. While Al-Akraa et al. (2014) reported that the interosseous muscle appears on the palmar aspect of the metacarpal bone in both CT images and cross sections as an elongated or flattened structure in cattle and elliptical in buffalo. However, El-Shafey and Sayed-Ahmed (2012) in buffalo and camel observed this muscle more distinctly in cross sections than in the CT images.

The joint capsule of the fetlock appeared in this study with a low signal intensity, the margins of this capsule were clearly outlined as thin lines of intermediate signal intensities on the transverse, dorsal, and sagittal MR images. Similar findings were observed in the fetlock joint of cattle (Hagag and Tawfik 2018). Moreover, this capsule appeared as a hypodense structure on the transverse, dorsal, and sagittal CT images, similar to the findings of El-Nahas et al. (2015) in camel. On contrary, this joint capsule cannot be observed using the CT or MR images, due to they are potential cavities appear only in linear cross sections (El-Shafey and Abd Al-Galil 2012 in camel; El-Shafey and Kassab 2012 in camel and buffalo; Al-Akraa et al. 2014 in cattle and buffalo).

5. Conclusion

The current study provided definite anatomical cross sections with their corresponding CT and MR images of the most clinically relevant structures of the fetlock joint in dromedary camel. These images

could be used as a normal anatomic reference during the diagnosis of the musculoskeletal disorders in this region.

6. Conflict of interest

The authors have no conflict of interest to declare

7. References

- Abedallaah B, Awaad AS, Elhawari SF, Sharshar AM (2015). Normal brain of one humped camel: a study with magnetic resonance imaging and gross dissection anatomy. *Indian Journal of Veterinary Surgery*, 36(1): 46-50.
- Ahmad S, Yaqoop M, Hashmi M, Ahmad S, Zaman MA, Tariq M (2010). The economic importance of camel: A unique alternative under crisis. *Park Vet. J.*, 30(4): 191-197.
- Al-Akraa AM, El-Kasapy AH, El-Shafey AA (2014). Intra-articular injection, computed tomography and cross sectional anatomy of the metacarpus and digits of the cattle (*Bos taurus*) and buffalo (*Bos bubalis*). *Global Veterinaria*, 13(6): 1122-1128.
- Al-Juboori A (2013). Prevalence and etiology of lameness in racing camels (*Camelus dromedarius*) in Abu Dhabi Emirate. *Journal of Camelid Science*, 6: 116–121.
- Arencibia A, Vazquez JM, Rivero M, Latorre R, Sandoval JA, Vilar JM, Ramirez JA (2000). Computed tomography of normal cranioccephalic structures in two horses. *Anat. Histol. Embryol.*, 29: 295–299.
- Badawy AM (2011). Computed tomographic anatomy of the forefoot in one humped camel (*Camelus dromedaries*). *Global Veterinaria*, 6(4): 417-423.
- Bienert A, Stadler P (2006): Computed tomographic examination of the locomotor apparatus of horses a review. *Pferdeheilk.*, 22: 218-26.
- Cohen ZA, McCarthy DM, Kwak SD, Legrand P, Fogarasi F, Ciaccio EJ, Ateshian GA (1999). Knee cartilage topography, thickness, and contrast areas from MRI: In-vitro calibration and in vivo measurements. *Osteoarthritis and Cartilage*, 7: 95-109.
- Denoux JM, Crevier N, Roger B, Lebas JF (1993). Magnetic resonance imaging of the equine foot. *Veterinary Radiology and Ultrasound*, 6: 405-411.

- El-Nahas A, Hagag U, Brehm W, Ramadan RO, Al Mubarak A, Gerlach K (2015).** Computed tomography of the hind limbs in healthy dromedary camel foot. *U. of K. J. Vet. Med. Anim. Prod.*, 6(2): 98-102.
- El-Shafey AA, Abd Al-Galil ASA (2012).** Magnetic resonance image of the one humped (*Camelus dromedarius*) digits. *Journal of American Science*, 8(9): 549-556.
- El-Shafey AA, Kassab A (2012).** Computed tomography and cross sectional anatomy of the metatarsus and digits of the one humped camel (*Camelus dromedaries*) and Egyptian water buffalo (*Bos bubalis*). *Anat Histol Embryol.* 42: 130-137.
- El-Shafey AA, Sayed-Ahmed A (2012).** Computed tomography and cross sectional anatomy of the metacarpus and digits of the one humped camel and Egyptian water buffalo. *Journal of American Science.* 8(9): 549-556.
- Farah Z, Fischer A (2004).** Milk and meat from the camel: Handbook on products and processing publishing. Zurich, Switzerland: ETH Univ. Publishing. Hochschuleverlang AG ander ETH Zurich, pp15-28.
- Hagag U, Tawfik MG (2018).** Ultrasonography, computed tomography and magnetic resonance imaging of the bovine metacarpo/metatarsophalangeal joint. *The veterinary Journal*, 233: 66-75.
- Kinns J, Nilson N (2010).** Imaging tarsal trauma. *Equine Veterinary Education*, 22(6): 296-298.
- Lisher CJ, Kishimoto U (2005).** Fracture of the para condylar process in four horses: advantages of CT imaging. *Equine Veterinary Journal*, 37(5): 483-487.
- Nuss K, Schnetzler C, Hagen R, Schwarz A, Kircher P (2011).** Clinical application of computed tomography in cattle. *Tierarztl PraxAusg G Grosstiere Nutztiere*, 39: 317- 324.
- Onar V, Kahvecioglu KO, Cebi V (2002).** Computed tomography analysis of the cranial cavity and neurocranium in the German shepherd dog (Alsatian) puppies. *Veterinary Archive*, 72: 57-66.
- Pollard R, Puchalski S (2011).** CT contrast media and applications. In: *Veterinary computed tomography*. Schward, T. and Saunders J. (eds), Willey-Blackwell, pp 57- 65.
- Puchalski SM, Galuppo LD, Hornof WJ, Wisner ER (2007).** Intra-arterial contrast-enhanced computed tomography of the equine distal extremity. *Veterinary Radiology and Ultrasound*, 48(1): 21-29.
- Raji AR, Sardari K, Mohammadi HR (2008).** Normal cross-sectional anatomy of the bovine digit: comparison of computed tomography and limb anatomy. *Anat Histol Embryol.* 37: 188-191.
- Raji AR, Sardari K, Mohammadi HR (2009).** Magnetic resonance imaging of the normal bovine digit. *Veterinary Research Communication*, 33: 515-520.
- Sadegh BAM, Shadkhast S, Sharifi A, Mohammadnia HR (2007).** Lacrimal apparatus system in one humped camel of Iran (*Camelus dromedarius*): Anatomical and radiological study. *Iranian Journal of Veterinary Surgery*, 2(5): 76-80.
- Samii VF, Briller DS, Kobic PD (1998).** Normal cross-sectional anatomy of the feline thorax and abdomen: comparison of computer tomography and cadaver anatomy. *Veterinary Radiology and Ultrasound*, 39: 504-511.
- Sampson SN, Schmeider RK, Tucker RL (2005).** Magnetic resonance imaging of the equine distal limb.in: equine surgery. 3rd ed. Auer JA, Stick JA (eds) Philadelphia: Saunders, pp 946-963.
- Sampson SL, Tucker RL (2007).** Magnetic resonance imaging of the proximal metacarpal and metatarsal regions. *Clinical Technical Equine Practice*, 6: 78-85.
- Seddek AM, Abedellaah BA, Awaad AS (2014).** Computed tomography and dissection anatomy of the frontal and maxillary sinuses in native Egyptian goats. *Indian Journal of Veterinary Surgery*, 35(1): 12-16.
- Smith MA, Dyson SJ, Murray RC (2011).** The appearance of the equine metacarpophalangeal region on high-field vs standing low-field magnetic resonance imaging. *Vet. Radiology and Ultrasound*, 52: 61-70.
- Solano L, Barkema HW, Pajor EA, Mason S, LeBlanc SJ, Zaffino-Heyerhoff JC, Nash CG, Haley DB, Vasseur E, Pellerin D (2015).** Prevalence of lameness and associated risk factors in Canadian Holstein-Friesian cows housed in free stall barns. *Journal of Dairy Science*, 98: 6978–6991.
- Vanderperren K, Ghaye B, Hoegaerts M, Saunders JH (2008).** Evaluation of Computed Tomographic Anatomy of the Equine

metacarpophalangeal Joint. American Journal of Veterinary Research, 69: 631-638.

Vand Der Vekens E, Gergman EH, Van Der veen H, Vanderperren K, Raes EV, Puchalski SM, Bree HJ, Saunders JH (2011). Computed tomographic anatomy of the equine stifle joint. American Journal of Veterinary Research, 72: 512-521.

Young BD, Samii VF, Mattoon JS, Weibrode SE, Bertone AL (2007). Subchondral bone density and cartilage degeneration patterns in osteoarthritic metacarpal condyles of horses. American Journal of Veterinary Research, 68: 841-849.